



Magnetotelluric and aeromagnetic investigations for assessment of groundwater resources in Parnaíba basin in Piauí State of North-East Brazil

E. Chandrasekhar^{a,b,*}, Sergio L. Fontes^b, Jean M. Flexor^b, Mita Rajaram^c, S.P. Anand^c

^a Department of Earth Sciences, Indian Institute of Technology Bombay, Powai, Mumbai-400076, India

^b Departamento de Geofísica, Observatório Nacional-MCT, Rua General José Cristino 77, São Cristóvão, CEP 20921-400, Rio de Janeiro, Brazil

^c Indian Institute of Geomagnetism, New Panvel, Navi Mumbai-410218, India

ARTICLE INFO

Article history:

Received 26 October 2007

Accepted 11 December 2008

Keywords:

Parnaíba basin

NE Brazil

Groundwater

Magnetotellurics

Aeromagnetism

ABSTRACT

In an attempt to locate the presence of possible groundwater resource regions in the semi-arid North-East Brazil, an integrated survey including aeromagnetic and magnetotelluric (MT) studies have been undertaken in the Guaribas region and only MT survey in the Caracol region. In the Guaribas region the aeromagnetic data, its analytic signal and Euler solutions reveal several subsurface small-scale faults and intrusives that are conducive to be potential groundwater resource regions. A total of about 22 broad-band magnetotelluric (MT) soundings in the period range of 0.006–300 s along two profiles on the marginal arcs of the intra-cratonic sedimentary Parnaíba basin in North-East Brazil have been made across the regional geological strike, the Senador Pompeu Lineament (SPL). SPL trends N40°E and marks a basement high reflecting an irregularity in the original basin geometry. While one of the MT profiles traverses across the SPL, the other lies only in the aeromagnetically surveyed sedimentary region. Two-dimensional inversion of MT data of both profiles shows that the sedimentary basin is conductive (100–150 Ω m) and shows as a thin graben with an average thickness of about 2–3 km beneath both profiles. The basin is located to be at shallow depths (from surface to about 500 m). Based on the facts that the study region falls on sedimentary region having low-to-very low permeability and also in accordance with the subsurface lithology around the study region, the mapped sedimentary basin largely manifests the zone of potential sedimentary aquifer having moderate resistivity of 50–250 Ω m and is located at relatively shallow depths. The identified aquifer zone is believed to have links with the Parnaíba River flowing at a distance of about 300 km NW from the study region. We discuss interpretation of our results of MT and aeromagnetic data sets in the light of hydrological features of the study region.

© 2008 Elsevier B.V. All rights reserved.

1. Introduction

The major tectonic reactivation of the Brazilian shield is linked to the structures developed during the Brazilian Orogenic cycle (750 to 550 Ma) during the Precambrian. Another key aspect of the Precambrian tectonic framework is the evolution of the Trans-Brazilian Lineament (TBL) (Schobbenhaus et al., 1975). TBL trends N45°E and spans about 2700 km across the Brazilian territory, connecting some lineaments in Paraguay and Argentina (de Brito Neves, 1991). Later, by the end of Silurian, subsidence at several places in Brazil had resulted in the formation of three major intra-cratonic sedimentary basins; the Amazon in the NW, the Parnaíba in the NE and the Parana in the South. The inset in Fig. 1 shows a schematic representation of these intra-cratonic basins of Brazil (after de Sousa, 1996). The marginal arcs and subsequent sedimentation of all these basins were fully developed by late Devonian of middle Paleozoic with

differential rates of sedimentation (de Sousa, 1996). A notable geological sequence that followed later was the inter-connection of all these basins during the largest marine transgression that had occurred in Paleozoic era. As a result, marine sediments were found in Parnaíba and Amazon basins up to Upper Carboniferous and up to Permian in the Parana basin (de Sousa, 1996). In the present work, we focus only on the Parnaíba basin – the region of present study.

The Parnaíba basin is oval in shape and spans the entire region by about 1000 km in NW and by about 800 km in SE. Fig. 1 displays the tectonic and structural settings of the Parnaíba basin and its contiguous regions, in the Piauí state of NE Brazil (after de Sousa, 1996). The TBL (see Fig. 2 for its location) controls the evolutionary history and shape of the basin. It is composed of small-scale faults and dykes cutting the geological units of distinct periods and is related to several basement grabens towards NE and SW ends of the basin (Cunha, 1986). Contrary to its dimensions, the basin is very thin and is mainly composed of Paleozoic sediments of Serra Grande and Caninde groups of Silurian and Devonian. The lithology in and around the East and SE margins (the present study region) of the Parnaíba basin is mainly composed of alternating sequences of thin layers of shales,

* Corresponding author. Department of Earth Sciences, Indian Institute of Technology Bombay, Powai, Mumbai-400076, India. Tel: +91 22 2576 7257; fax: +91 22 2576 7253. E-mail address: esekhar@iitb.ac.in (E. Chandrasekhar).

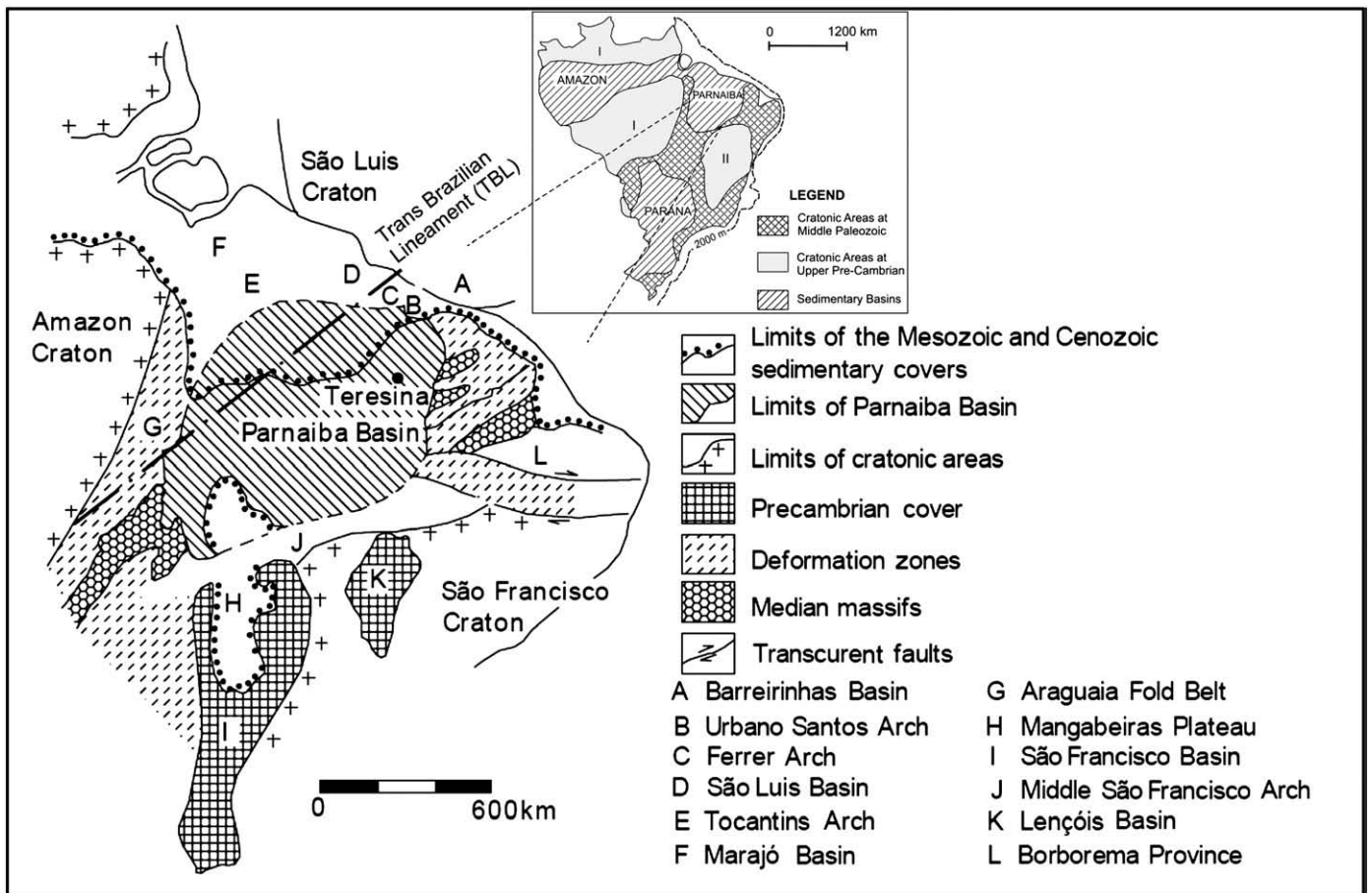


Fig. 1. Tectonic and structural settings of Parnaíba basin and other contiguous regions, in Piauí state of NE Brazil (after de Sousa, 1996). Inset shows the schematic description of intracratonic basins of Brazil (after de Sousa, 1996).

siltstones, coarse-to-fine sandstones, quartz pebbles, conglomerates, etc (see Fig. 2 of Meju et al. (1999) for more lithostratigraphic details). Coupled with such a lithology, the tectonic setting of the Parnaíba basin, formed with marine sediments, aptly facilitate the formation and setting up of an environment favourable for potential groundwater resources. Since the region under investigation forms a natural laboratory for groundwater assessment studies, a high resolution mapping of subsurface geologic units with interfaces between sediments and the underlying basement is essential.

Owing to their ease of use, electromagnetic and electrical resistivity methods, for assessment and exploration of groundwater resources have been studied for over two decades (for e.g., see Palacky et al., 1981; Stewart, 1982; Fitterman and Stewart, 1986; McNeill, 1987; Sandberg, 1993). Meekes and Van Will (1991) have compared seismic reflection and resistivity sounding data for groundwater assessment. Chouteau et al. (1994) and Giroux and Chouteau (1997) analyzed magnetotelluric (MT) data to characterize the Santa Catarina aquifer systems in Mexico basin and the Maestrichtian aquifer system in Senegal, Africa, respectively. Meju and Fontes (1996) and Meju et al. (1999) have described joint analyses of resistivity sounding, TEM and Audio magnetotelluric techniques for groundwater assessment in semi-arid regions. Later Krivochieva and Chouteau (2003) further improved the characterization of Santa Catarina aquifer system by integrating the time-domain electromagnetic (TDEM) and MT data. Meju et al. (1999) have also provided a quantitative estimation of the groundwater yield in the eastern margins of the Parnaíba basin. In fact, there are several unexplored regions, where isolated pockets of groundwater resource regions in SW and SE portions of the Parnaíba basin are believed to exist in the moderately populated villages, suffering with water scarcity.

With a view to fill this gap, MT and TEM surveys have been conducted in the year 2003 in Guaribas and Caracol regions in SE marginal arcs of Parnaíba basin, with both objectives of identifying the subsurface target areas having low resistivity contrasts from the surrounding environment and estimating the target depths for agricultural and rural development. An aeromagnetic survey was also conducted in the Guaribas region by Fugro (an International commercial company for airborne geophysical surveys). Both MT and aeromagnetic studies cover a small region on the marginal arcs of the semi-arid Parnaíba basin, in SE portion of Piauí State. In this paper we first explain the analysis of aeromagnetic data to look for viable hydrogeological areas (Section 2) and then describe the processing and analysis of MT data of two profiles (Section 3) and finally discuss the results and interpretation of both the data sets (Section 4) in the light of the above objectives.

2. Aeromagnetic data analysis

High resolution three-component aeromagnetic data: horizontal north-south, X , horizontal east-west, Y , vertical component, Z and total field (F) were collected along 41 parallel profiles oriented $N28^{\circ}W$ at an altitude of 100 m with an inter-profile distance of 500 m in Guaribas region by Fugro in 2003. The small rectangular box within the inset of Fig. 2 shows the area of aeromagnetic data coverage in Guaribas region. Cesium vapour airborne magnetic sensors of model CS-3 Scintrex, having a sensitivity of 0.001 nT were used for recording the data.

Groundwater in sedimentary rocks is generally encountered in cracks, fissures, bedding planes, pore spaces and contact zones with intrusions. Hence it is necessary to look for these features in the

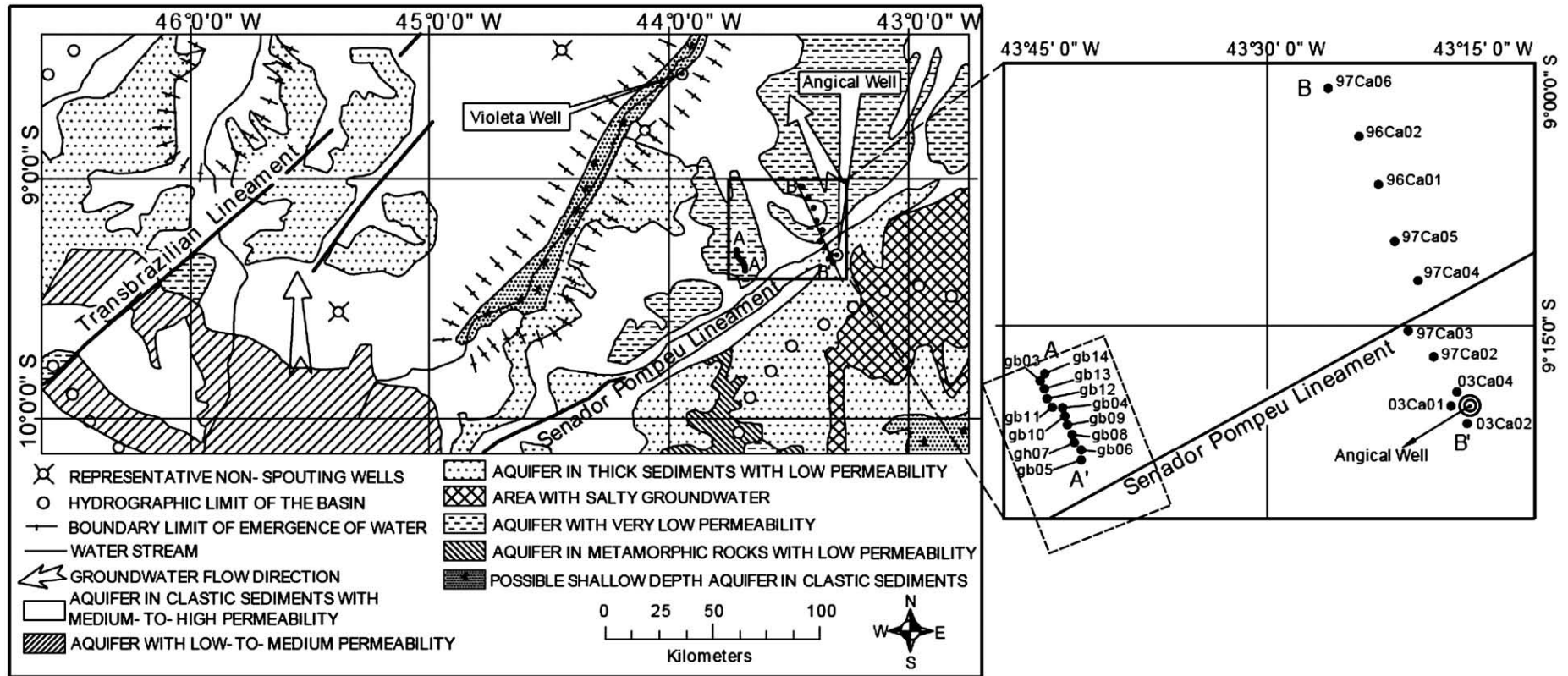


Fig. 2. Location of MT sites of Guaribas region (profile AA') and Caracol region (profile BB') shown on the background of hydrogeological map of the Parnaíba basin along with the adjoining tectonic setting and different types of aquifer zones. Within the inset, the region covered under aeromagnetic survey is shown as a tilted and dashed rectangle over AA' profile. The Trans-Brazilian Lineament (TBL), which is the major source for the tectonic reactivation of the Brazilian shield during the Precambrian, is also shown in the figure. The Senador Pompeu Lineament (SPL), running parallel to TBL marks the regional geologic strike trending N40°E. The SPL marks the basement high.

aeromagnetic anomaly map. A model suggested by Babiker and Gudmundsson (2004) predicts that water wells and springs would be expected at dyke–fault intersections. Therefore, the main aim of the analysis of the airborne magnetic data was to identify dykes, faults and to check the locations where they intersect and to study the available MT survey data within this region (profile AA' in Fig. 2) to exactly delineate possible groundwater resource regions. We have processed aeromagnetic data using the commercial software, Oasis Montaj™. Aeromagnetic total field (F) data were corrected using IGRF 2000 coefficients (obtained from <http://www.ngdc.noaa.gov/IAGA/vmod/igrf.html>) for removing the Earth's main field component from the data. The total field anomaly map of the region is shown in Fig. 3. Several NW–SE structural trends can be seen within the basin proper that may possibly represent fragments of small-scale faults and/or dyke-like structures as the basin proper is mainly composed of shales, sandstones, quartz and conglomerates, which are essentially non-magnetic. These small-scale structural features appear to be abruptly terminated at the SPL which manifests itself as a NE–SW trending structure associated with long wavelength anomalies.

The magnetic inclination and declination of the study region are -16.5° and -23° respectively. Therefore a direct interpretation of the total field anomaly map can be erroneous in such low latitude regions (Rajaram, 2003). Independent of the geomagnetic latitude, the analytic signal map of the total field can delineate the magnetic sources (Roest et al., 1992). Therefore, to have a better understanding of the distribution of magnetic sources (mainly shallow sub-surface intrusives), an analytic signal map is prepared (Fig. 4). The highs (red colour) in Fig. 4 overlie the magnetic sources. From the nature of the

NW–SE trending highs in the analytic signal map it appears that most of the sources as seen within the basin proper represent intrusives/diabase dykes. To understand the nature and depth of the faults in the study region, the Euler deconvolution method (Thompson, 1982) is applied to the gridded data (Reid et al., 1990). Euler's homogeneity equation relates the magnetic field and its gradient to the location of the source of an anomaly, with a certain degree of homogeneity, expressed as structural index (SI). SI relates to the type of source causing the anomalies and signifies the measure of the fall-off rate of the field with distance from the source. For example, Reid et al. (1990) have explained that the magnetic field of a point dipole falls off as the inverse cube, giving an index of three; a vertical line source (such as a narrow vertical pipe), gives rise to an inverse square field fall-off and an SI of two; similarly, extended bodies are assemblage of dipoles and have SIs varying from 0 to 3, while $SI = 0$ represents a fault/contact. The reliability of solutions is gauged by their good clustering and accordingly, the corresponding SI is chosen. A proper choice of SI is very important for correct/accurate estimation of Euler depths. Although these integer values represent an ideal relationship between structural index and source type, for real data, the source could be represented by a structural index that can take any real (non-integer) value between 0 and 3. The optimum source location is found by least squares inversion of the data within a chosen window length. Solutions are generally obtained for different $SI = 0, 0.5, 1.0, 1.5, 2.0, 3.0$ and the solutions with the best clustering of data are selected. The correct SI for a given feature is that which gives the tightest clustering of solutions. From this, one can think of SI as a focus control, in which the correct SI produces the sharpest focus of results. Since our aim was

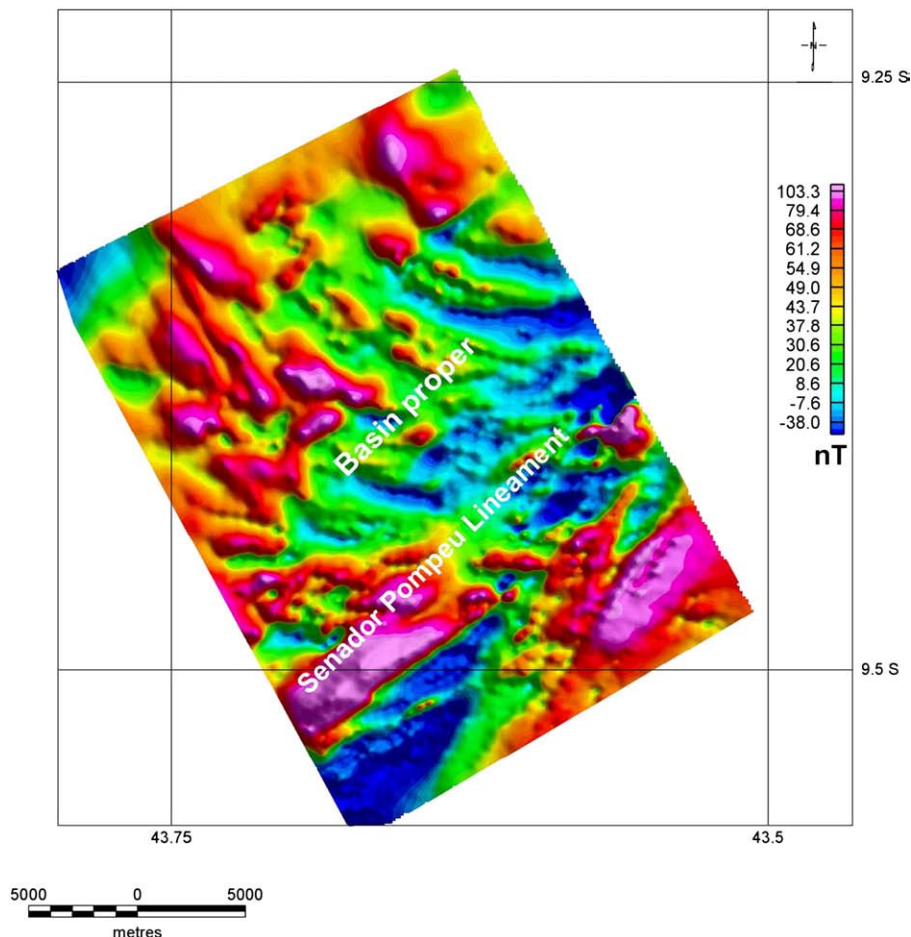


Fig. 3. The aeromagnetic total field anomaly map generated after removing the main field component using IGRF 2000 coefficients.

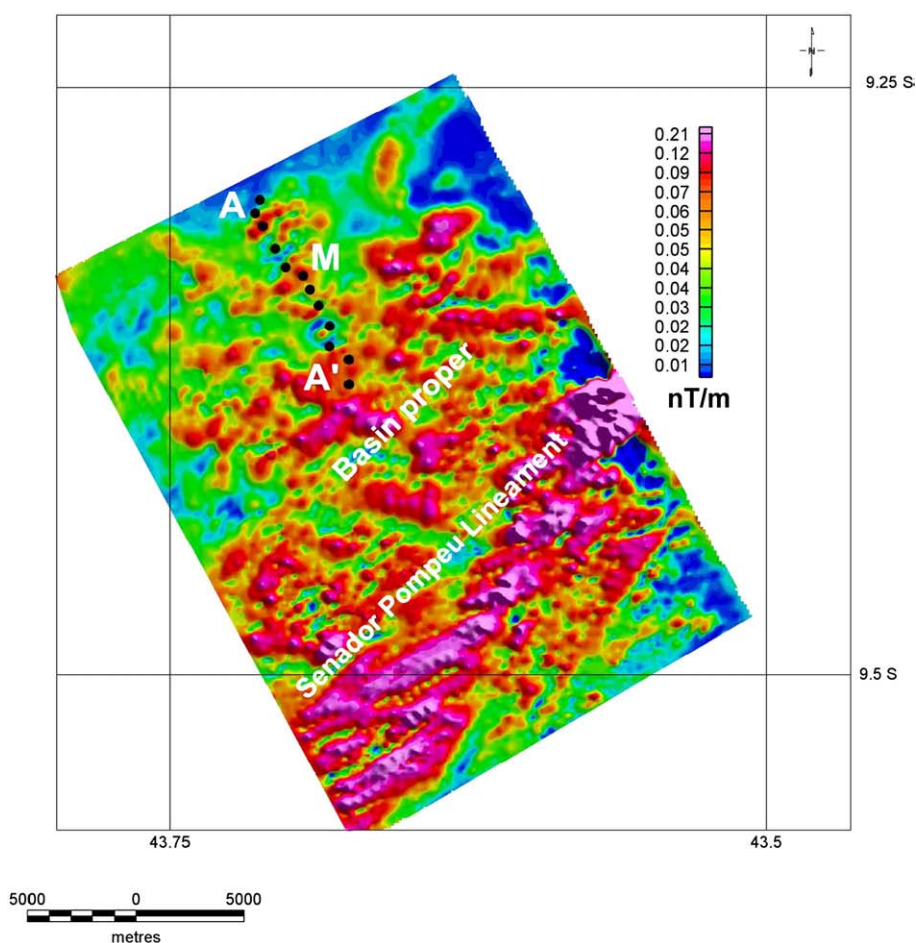


Fig. 4. Analytic signal map of the aeromagnetic data depicting major magnetic sources (red coloured zones). The region 'M' is traversed by relatively deep NW–SE faults cut by relatively shallow NE–SW faults with no major magnetic sources within the sedimentary basin above the basement. Black dots indicate the MT profile AA'.

to delineate the faults from the anomaly map, we have calculated Euler solutions using window length of 10 for $SI=0$ and 0.5, which represent fault/contacts. For calculating the Euler solutions, we have used anomaly data that was continued upward to 500 m as the total field anomaly data (Fig. 3) is contaminated with high frequency noise. The errors associated with the source depths of Euler solutions thus generated are $\leq 15\%$ and the errors in their spatial location on the surface is $\leq 25\%$. Fig. 5 reproduces the Euler solutions obtained after upward continuation to 500 m for $SI=0$, representing faults/contact. The source depths of Euler solution are represented by different coloured circles. The colour scale in Fig. 5 denotes the depth estimates of the Euler solution. Several faults trending NW–SE, NE–SW, EW can be seen in Fig. 5. Apart from the several faults, the SPL, which is a contact between the crystalline basement and the sedimentary basin, is very well brought out.

We have made an attempt to locate the regions within the basin proper where the faults intersect the intrusives. Some of the identified locations are marked with numbers, 1,2,...,7,8, in Fig. 5. The present analysis suggests that several faults which intersect the dykes/intrusives lie in the subsurface, which sets up an environment favourable for groundwater accumulation (Babiker and Gudmundsson, 2004). The fault zones identified in the Euler solutions act as conduits for movement of water that can be trapped in the regions where they intersect the dykes. In Fig. 4, the region marked as 'M' is traversed by relatively deep NW–SE faults cut by relatively shallow NE–SW faults with several shallow magnetic sources within the sedimentary column above the basement thus forming a potential zone for ground water accumulation. The MT Profile AA' lies in this region and a detailed study of this data is carried out to locate the presence of any ground water

accumulation zones. It may be noted that this profiles falls in the region representing aquifer with very low permeability (Fig. 2).

3. MT data acquisition and processing

A total of 22 broad-band five-channel MT soundings in the period range of 0.006–300 s were acquired using EMI MT-1 equipment in 2003 along two profiles, Guaribas (AA') and Caracol (BB'). There are 12 stations along AA' and 10 along BB' profile with an inter-station spacing of 1 km and 4 km respectively. Along the BB' profile, MT survey was first done in 1996–97 and a repeat survey was done in 2003. In the present study we have used data sets of both these campaigns. Fig. 2 shows the location of MT profiles superposed on the hydro-geological map of the study region. Both AA' and BB' were laid perpendicular to the regional geological structure, the Senador Pompeu Lineament (SPL). SPL marks the basement high reflecting the irregularity in the basin geometry, which appears as if it is splitting the sedimentary Parnaiba basin structure. The SPL, which trends $N40^{\circ}E$ (and parallel to the TBL), is not currently tectonically active. While AA' lies within the sedimentary region, BB' traverses across the SPL (see inset of Fig. 2). The inter-profile distance is about 45 km. We have processed the measured data using the robust processing code of Egbert (1997). For most stations of both profiles, MT data are in general two-dimensional (2-D) in the period range 0.01–10 s.

3.1. Determination of strike angle

Following the sequential procedure outlined by Groom et al. (1993) we have decomposed MT impedance tensor elements to constrain the

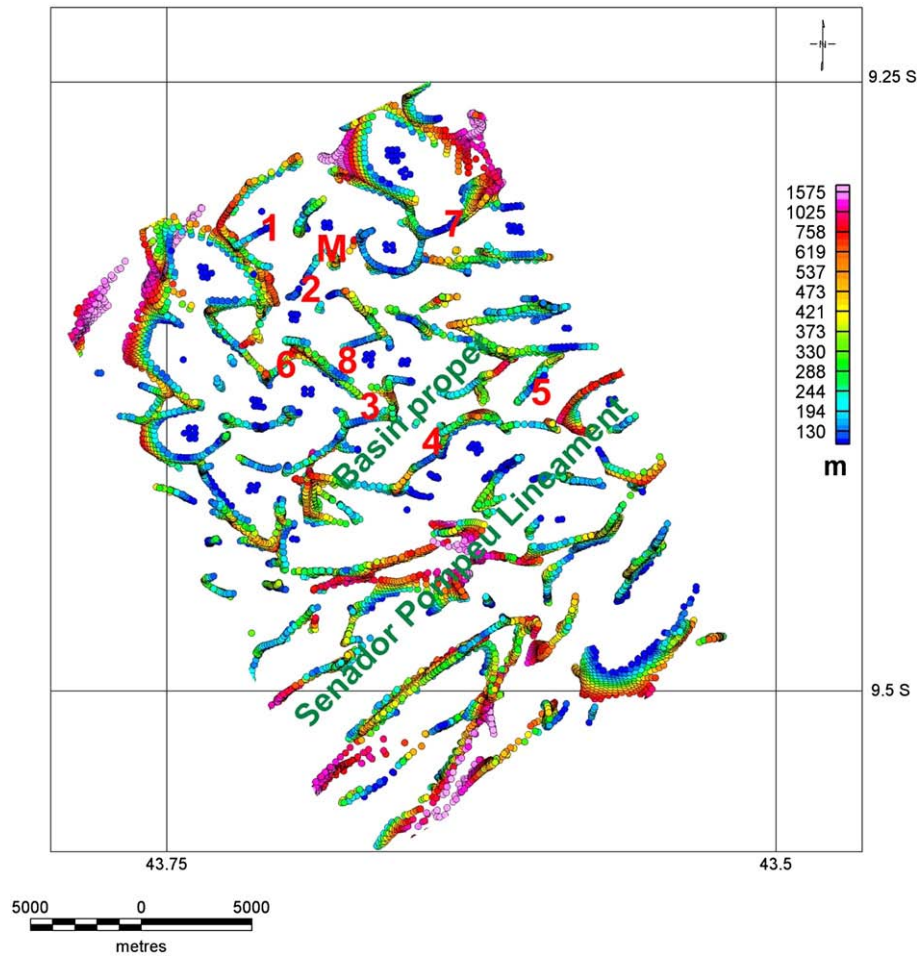


Fig. 5. Location and depth of major faults in the region obtained using Euler deconvolution method for $SI = 0$ representing fault/contact with window length = 10. The scattered numbers (1 to 8) indicate locations of several faults, which intersect the dykes/intrusives in the subsurface.

galvanic distortion parameters: shear, twist and strike (Groom and Bailey, 1989) using the 'strike' program of McNeice and Jones (2001). First, for the unconstrained decomposition, the distortion parameters were allowed to freely vary within their physical limits, i.e., -45° to $+45^\circ$ for shear, -60° to $+60^\circ$ for twist and -90° to $+90^\circ$ for strike. The procedure followed for determination of strike angle at each station of AA' profile is explained below. From the plots of unconstrained decomposition, first the variation of shear and twist angles with period was checked. If either of these was found to be stable (period independent) in a certain period range, then first, that parameter was constrained to its average value in that period range. Then next the other parameter, and finally the strike were constrained in a similar fashion. It is generally advised that strike be constrained last. Our data showed that shear and twist angles are relatively stable in the period range 0.1–1 s but beyond 10 s, both are highly scattered. This has been the nature of data at most of the stations. The distribution of finally constrained shear and twist angles of all the stations along the profile AA' is shown in Fig. 6A. The shear and twist angles lie within the range of $\pm 15^\circ$, except at stations gb13 and gb03, where the distortion of the impedance tensor is significantly high. The existence of not so negligible values of twist and shear in the data at short periods suggests the presence of near-surface inhomogeneities, which severely affect the amplitudes of the impedance tensor elements.

Following the above described systematic procedure, we have obtained individual strike angles for each station. The calculated geoelectric strike angles showed $\pi/2$ ambiguity. The confusion about the correct strike estimation was overcome by calculating the tipper

strike angle at each station, as this does not show any ambiguity (Vozoff, 1991). The tipper strike directions (light arrows) are shown in Fig. 6B. The tipper strike angles at all stations are approximately parallel to the profile direction. Using the tipper strike angles, the $\pi/2$ ambiguity of the geoelectric strike is solved and the definitive geoelectric strike angles were obtained by rotating the impedance tensor of each station, perpendicular to tipper direction. The calculated tipper and geoelectric strike angles of AA' profile, are shown in Fig. 6B.

Strike angles estimated for stations of Caracol (BB') profile were not consistent with one another. It may be recalled here that MT data of two campaigns conducted in 1996–97 and 2003 have been used for analysis. Since AA' and BB' are very close to SPL, we expected the strike angles at stations of both profiles to be reasonably similar. However, contrary to our expectation, the calculated strike angles at BB' stations varied fairly from one station to the other. Therefore, to determine the optimum strike angle for this profile (which is expected to be consistent with that of AA' profile because of its close proximity to AA' profile) and to maximize the off-diagonal elements of the impedance tensor, we have rotated the impedance tensors of BB' profile to be parallel to that of AA' profile, which in turn is parallel to the regional geological strike, the SPL. The definitive final strike angle considered for both AA' and BB' profiles is $N40^\circ E$. For two-dimensional inversion (discussed below), the MT impedance tensor rotated in such a way that the magnetic (electric) field be parallel to the determined strike direction is regarded as the TM (TE) mode.

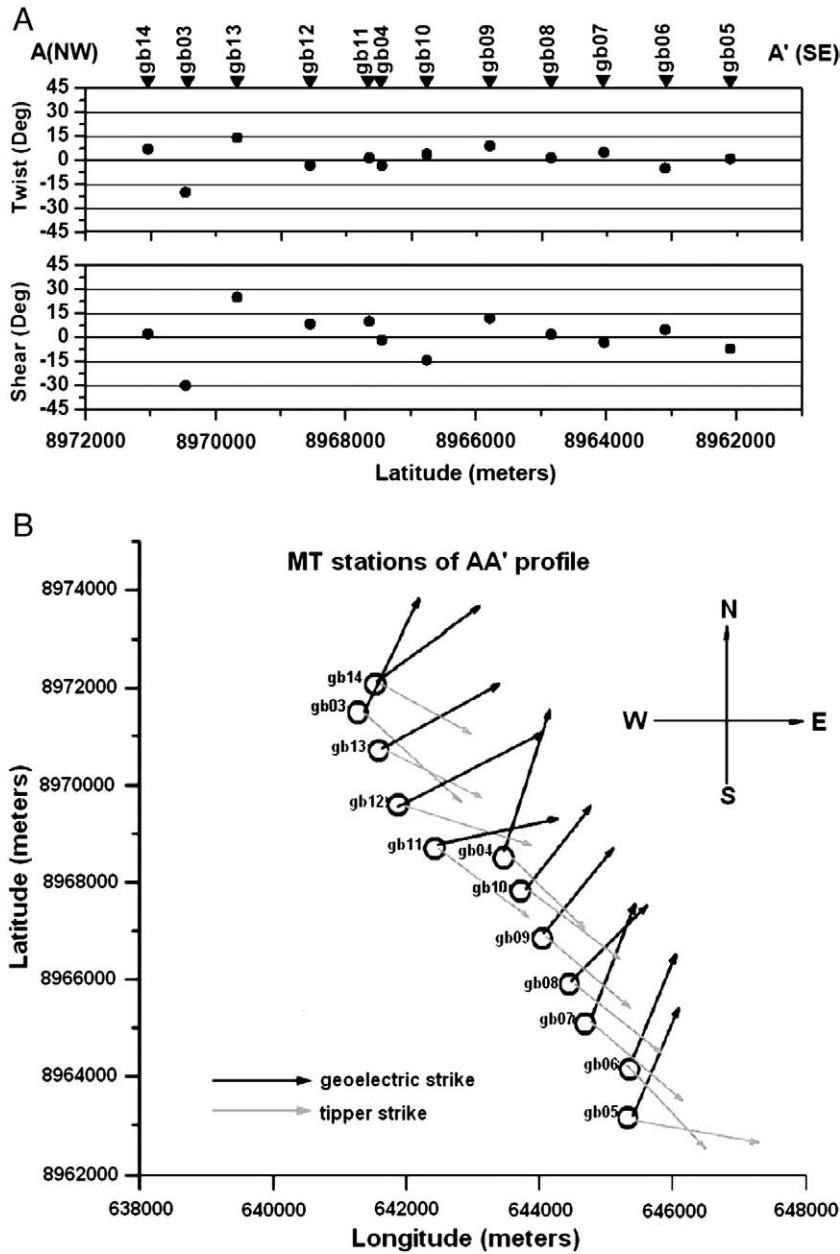


Fig. 6. Spatial distribution of estimated distortion parameters, Twist and Shear (A) and Tipper and strike angles (B) of AA' profile.

3.2. Static shift correction

A few stations showed static shift between the bimodal apparent resistivity data. TEM measurements at each representative site were also made in both single-loop and in-loop configurations with loop length of 50 m on each side. TEM data were used only to correct static shift effects in MT data, wherever necessary. Static shift between the bimodal MT apparent resistivity data is the consequence of the strong influence of subsurface galvanic distortions on the measured electric field at all frequencies. This restricts the true interpretation of MT data, if not corrected. On the other hand, the magnetic field is relatively unaffected by galvanic distortions. Therefore, use of magnetic field data, as detailed by Sternberg et al. (1988), is one of the effective ways to correct static shift in MT data. Several other methods, to remove static shift effects have been detailed by Jones (1988), Beamish and Travassos (1992), Singer (1992), Meju (1996, and references therein) and Ogawa (2002). Magnetic field data measured using controlled source TEM soundings at high frequencies (partly overlapping with

MT frequencies) at the co-located MT station have been inverted to get apparent resistivity (Sternberg et al., 1988; Pellerin and Hohmann, 1990). The 1-D inverted TEM data (called as pseudo-MT data) were then used to shift the observed MT apparent resistivity curves along the resistivity axis to match with the values suggested by pseudo-MT data. Fig. 7 depicts an example of the processed MT data of one of the stations, gb13 of AA' profile before (Fig. 7A) and after (Fig. 7B) removing the static shift effect.

3.3. Two-dimensional inversion

To determine the subsurface geoelectric structure beneath both the profiles, we have carried out two-dimensional inversion of data in the period range 0.01–10 s using the non-linear conjugate gradients algorithm of Rodi and Mackie (2001). We have jointly inverted the TE and TM apparent resistivity and phase data considering error floor of 10% on apparent resistivity and 5% on phase. The smoothing factor (τ) was set at 3. τ signifies the trade-off between data misfits and the

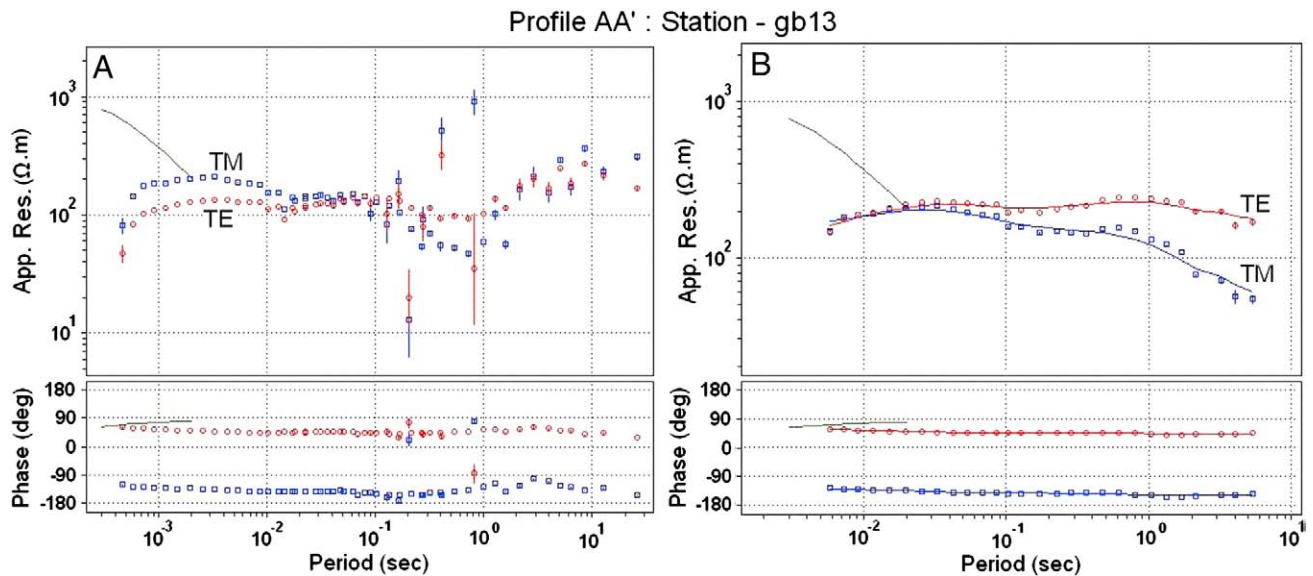


Fig. 7. An example of the processed MT data of one of the stations, gb13 of AA' profile (A) before and (B) after removing the static shift effect using TEM data. The two dimensional nature of the data representing TE and TM modes are shown. The solid lines (without symbols) designate pseudo-MT data in the high frequency range calculated using TEM data (Sternberg et al., 1988; Pellerin and Hohmann, 1990).

model smoothness. Larger values of τ help to generate smoother models, but at the expense of a worse data fit. Rodi and Mackie (2001) suggest that the τ should be set in the range of 3 to 300 for most MT 2-D inversions. However, it should optimally be so chosen, that the RMS error between the data and model lie between 1.0 and 1.5. In the present study, since we wanted to have as much best fit as possible between the data and model, we have set τ at its lowest value, 3. Figs. 8A and 9A show final geoelectric models for AA' and BB' profiles respectively, with an RMS fit between the data and model being 2.78 for AA' profile and 1.90 for BB' profile. Fig. 8B and C (Fig. 9B and C) show the pseudo-sections of the observed and calculated apparent resistivity and phase data corresponding to AA' (BB') profile. They respectively represent the pseudo-sections of TM and TE mode data. There is quite a good agreement between the observed and calculated data of both modes in each profile. It is pertinent to note here that on the pseudo-section plots, the measured data corresponding to those periods beneath each station as shown by dotted vertical lines should be considered relevant and any data shown beyond the periods corresponding to each station signify the interpolated values. However, such (interpolated) data are not used for interpretation of the results.

From the derived models, it is observed that TM mode data best fits the model, rather than TE mode data. This is true in the data sets of both the profiles. As well known, the galvanic noise produces a static shift effect if the data are 2-D. However, not having a good fit between the data and model particularly in case of TE mode should be associated with 3-D structures producing galvanic and inductive distortions.

The mapped sedimentary basin appears as a thin graben-like structure (average thickness of about 2–3 km) and is shallow (approximately 500 m deep) (Cunha, 1986). This is evident in Fig. 8A and is conductive (≈ 50 –250 Ω m). The conductivity of the basin is relatively high near the stations at the two ends of the AA' profile (marked as C1 and C2 in Fig. 8A), when compared to the conductivity of the whole basin (Fig. 8A). On comparison with Fig. 5 where we have marked some of the locations where the faults intersect the intrusives, we find that C1 is close to location 1 and C2 is close to location 8.

The derived model for BB' profile (Fig. 9A) clearly indicates a gradual thinning of the sedimentary basin as one traverses from NW end of the profile up to SPL (Fig. 9A). Further, it also shows that, in

agreement with the existing geology (see Cunha, 1986; Goes et al., 1993; de Sousa, 1996; Meju, 2006 (personal communication)), the average thickness of the sedimentary basin is about 2–3 km, beneath the part of the BB' profile that falls in the sedimentary region.

4. Discussion

Fig. 8A shows the geoelectric model for AA' profile obtained after jointly inverting the TE and TM mode data. The RMS error between the data and the model is 2.78 for this model. The model shows a thin conductive sedimentary formation with an average thickness of about 1–2 km, overlying a resistive basement (Cunha, 1986). Although the basin is located at very shallow depth, it is exposed to the surface at some places. While the basin comprises of alternating litho units of coarse-grained conglomerates, sandstones and fine-grained marine shales and siltstones, the basement comprises of schists, granites and gneisses, etc, which shows up as a single layer (Fig. 8A). The lithostratigraphic column of the Paleozoic sediments of the Parnaiba basin along with the well-log resistivity data (after Meju et al., 1999) are presented in the inset of Fig. 8A. The very good agreement of the mapped shallow sedimentary basin and its lateral extent with the lithology and the structure consisting of large-scale lineaments and small-scale faults/dykes in the study area suggests the mapped subsurface structure to represent a large-scale aquifer system.

From aeromagnetic data, the magnetic sources within the basin proper can possibly be related to the diabase dykes intruded into the basement as well as the sedimentary rocks. The network of faults, buried and interconnected underneath the sedimentary cover, has been clearly brought out by the Euler solutions calculated from the upward continued data (Fig. 5). Around the region marked as 'M' in the analytical signal map (Fig. 4), there are no major magnetic sources. It is bounded by fragments of several small-scale faults/fracture zones.

The mapped shallow sedimentary formation has been defined as a region having low permeability (see Fig. 2) (which could be due to lack of weathering (Fetter, 2001)), and agrees well with the lithology in and around the study region. It also holds a good correlation with the well-log resistivity data around the study region. A close comparison of well-log resistivity data and its corresponding lithology with the depth locations of the mapped sedimentary basin correspond to the very low-resistive Cabecas, Pimenteiras and Itaim sequences of

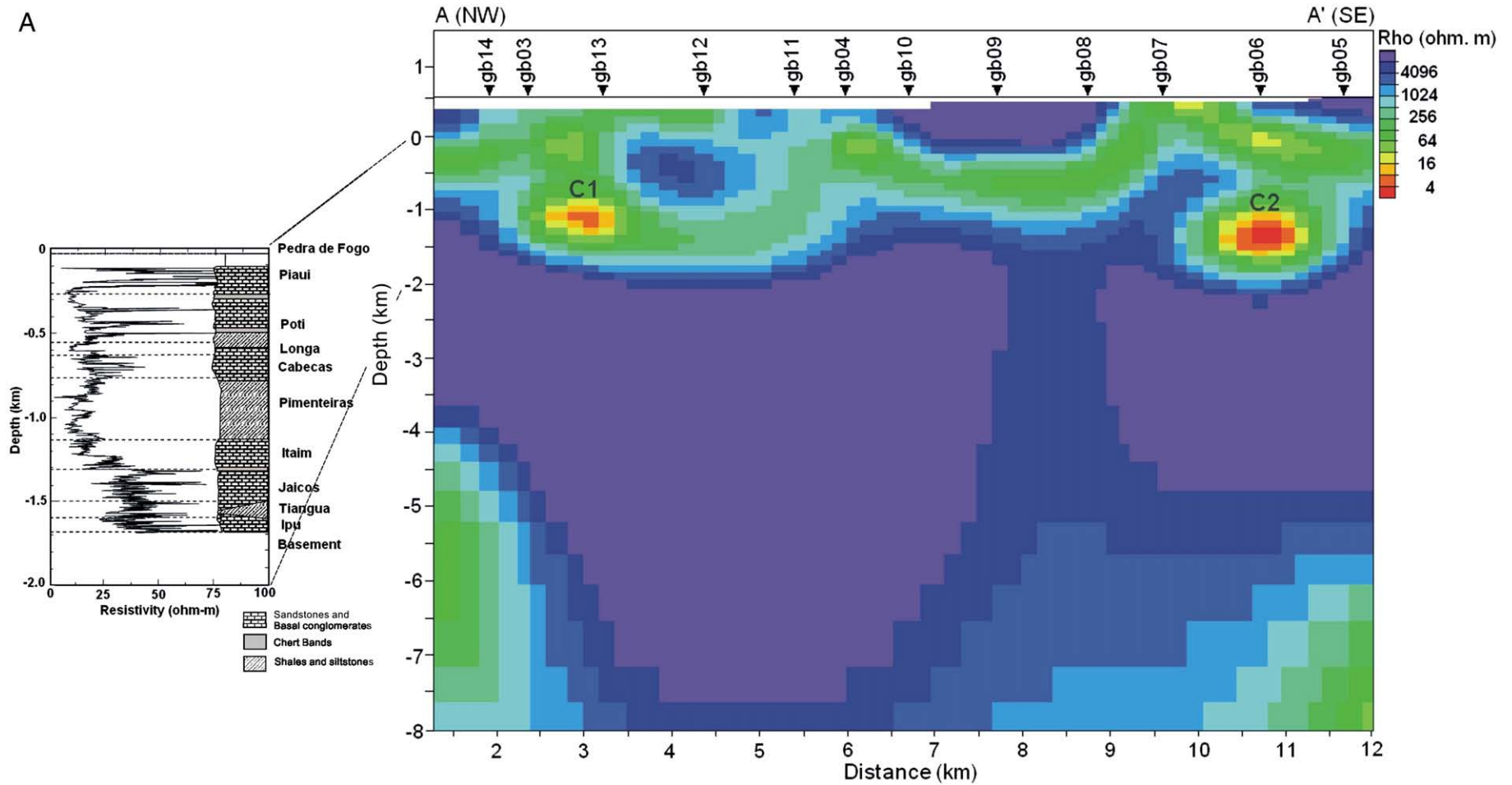


Fig. 8. Two-dimensional geoelectric model of MT data of (A) Guaribas (AA') profile. The model is obtained after jointly inverting the TE and TM mode data with error floor of 10% (5%) of apparent resistivity (phase). See text for description about C1 and C2. The RMS error for this model is 2.78. Inset shows the well-log resistivity data obtained from a place close to Guaribas region shown jointly with the lithostratigraphic column of the Parnaíba basin (after Meju et al., 1999). (B) and (C) describe the associated pseudo-section plots of the observed and calculated data for TM and TE modes respectively. In (B) and (C) the dotted vertical lines designate the measured data corresponding to those periods at each site.

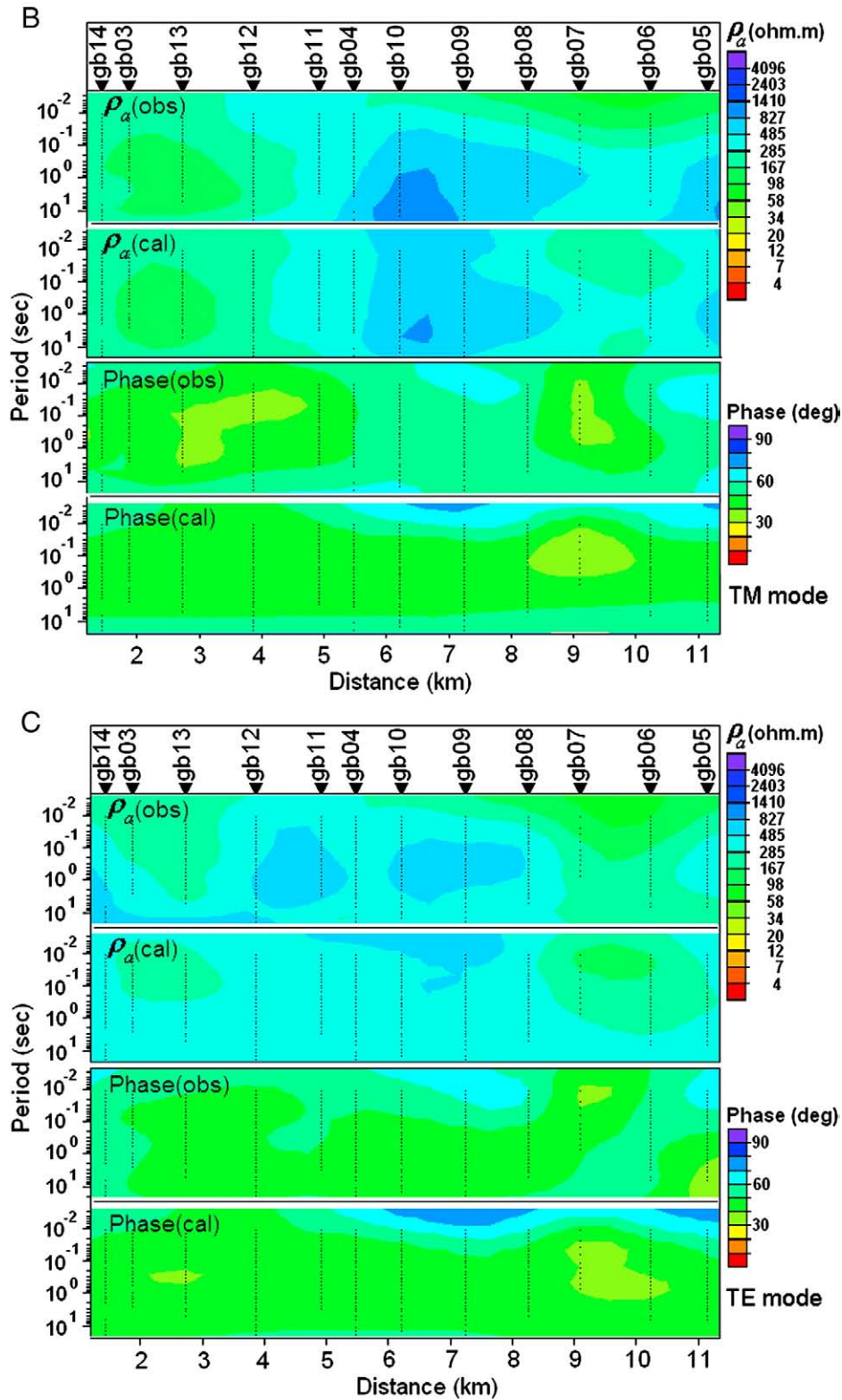


Fig. 8 (continued).

formations (see Fig. 2 of Meju et al., 1999). While the shaly and silty Pimenteiras, which are highly porous but less permeable, have very low resistivities, the Cabeças, Itaim, Jaicos and Ipu formations comprising of sandstone and quartz pebbles, having higher permeability than shales and siltstones, are the key lithologies that hold the groundwater. The two high conductivity zones located at almost same depths and marked as C1 and C2 in Fig. 8A probably represent the

porous but impermeable shales and siltstones that correspond to the very low-resistive Pimenteiras and Tiangua formations respectively. They are very low-resistive because they represent impermeable strata, containing stagnated water. Such comparative observations between well-log resistivity data, lithology of the study region and the derived geoelectric model strongly support and strengthen the accuracy of the estimated geoelectric model.

Fig. 9A shows the geoelectric model for BB' profile obtained after jointly inverting the TE and TM mode data. This profile traverses across the SPL (see Fig. 2). The RMS error between the data and the model is 1.9 for this model. This model also shows a thin sedimentary basin depicting different litho units, overlying a resistive basement. Beneath the part of the profile that falls in the sedimentary region, the average thickness of the basin is about 2–3 km, correlating well with the existing geology. Pseudo-section plots of apparent resistivity and phase data of TE and TM modes (Fig. 9B and C) clearly show the SPL as

a high resistive basement high. This is evident in Fig. 9A indicating that the conductive sedimentary basin appears to have split by the SPL and as a result, one can observe the gradual thinning of the sedimentary basin as one traverses from NW end of the profile up to SPL. This gives an impression that the resistive SPL may be interpreted as a basement high reflecting the irregularity in the original basin geometry. Based on such an interpretation of geoelectric model (Fig. 9A), a schematic of a feasible geological model has been illustrated in Fig. 10. The proposed geological model (Fig. 10) depicts a

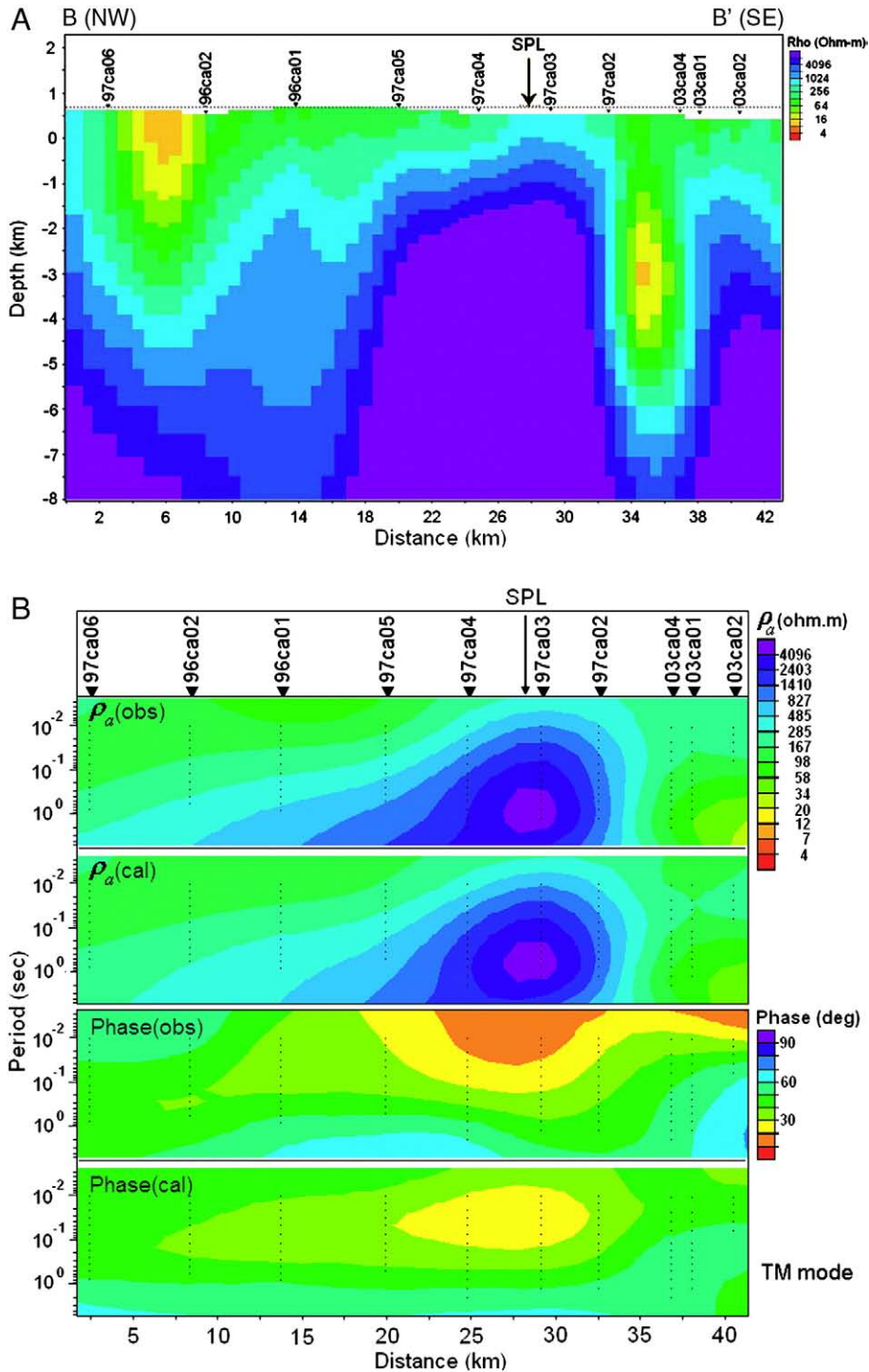


Fig. 9. Two-dimensional geoelectric model of MT data of (A) Caracol (BB') profile. The model is obtained after jointly inverting the TE and TM mode data with error floor of 10% (5%) of apparent resistivity (phase). The RMS error for this model is 1.9. The position of the regional geologic strike, the Senator Pompeu Lineament (SPL) is also shown. (B) and (C) describe the associated pseudo-section plots of the observed and calculated data for TM and TE modes respectively. In (B) and (C) the dotted vertical lines designate the measured data corresponding to those periods at each site.

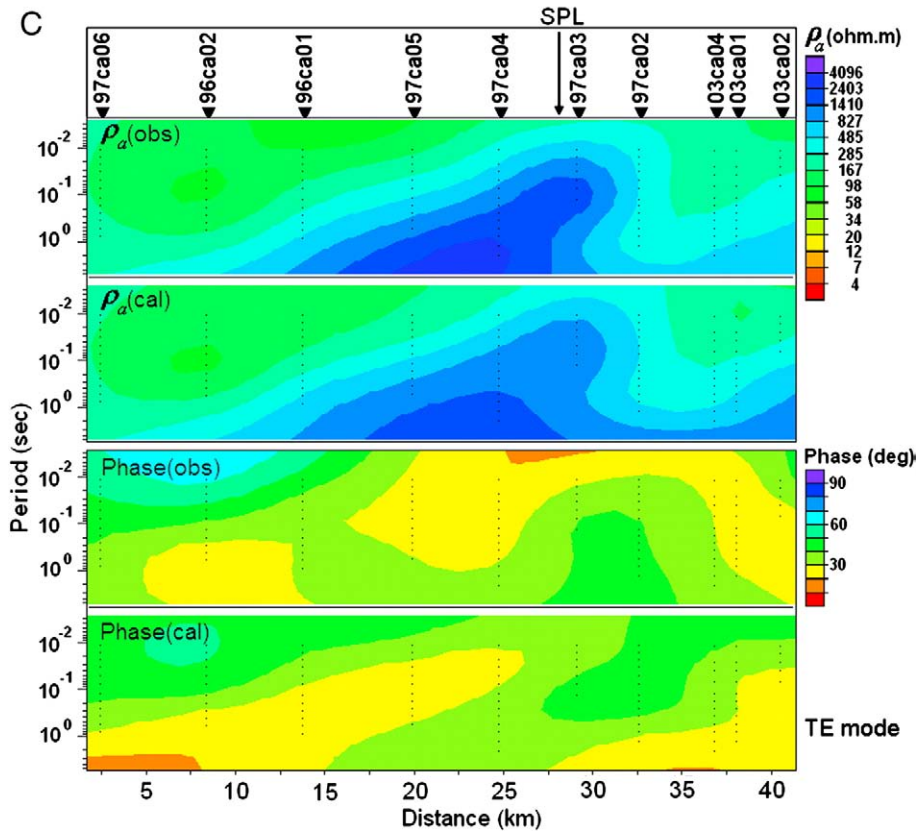


Fig. 9 (continued).

basement high representing the undulations in the basin geometry. However, additional MT data across the SPL are required to support this observation. Fig. 9A also shows shallow conductive sedimentary features exposed to the surface near both ends of the profile. It is not clear, whether these are artifacts of the model due to lack of measuring stations, or it may possibly be linked to the presence of Angical well (see Fig. 2) located close to SE end of BB'. The latter is particularly true for the conductive feature observed near the SE end of the profile. Further, the anomaly at the NW end of the profile falls in sedimentary region. Although this is correlated well with the basin lithology presented in the inset of Fig. 8A, we feel that since the distance between the two stations, 97ca06 and 96ca02 is more than 5 km, some more MT measurements must be made between these

two stations to confirm this. Only then such a comparison between the model and the lithology could be more meaningful and valid.

It can be seen that the spatial extent of the mapped aquifer in sedimentary formation is very large and that, if it is hydrogeologically linked to a recharge area, then it would serve as a potential aquifer. At a distance of about 100 km NW of AA' profile, there is a Violeta well (see Fig. 2), which has a yield of 900,000 L/h (CPRM (The Brazilian Geological service), personal communication). Such a high yield of this well indicates its hydrogeological linkage to a recharge area. Therefore, we tend to speculate that there may be a possibility for such a linkage of the mapped aquifer to a recharge area, particularly in view of the presence of Parnaiba river, flowing at a distance of about 300 km NW of AA' (not shown in Fig. 2) through a multitude of meandering faults and fractures of the Trans-Brazilian Lineament.

In spite of clear identification of presence of possible groundwater resources in Guaribas region, drilling is not possible at all places along the profile. For groundwater exploration, it is advisable that drilling at the NW end of profile (between the stations gb03 and gb13 (see Fig. 8A)) could be possible. It maybe noted here that the identified location "1" on the Euler solutions of the aeromagnetic data (Fig. 5) is very close to gb13. This is more feasible because in this region, the sediments are exposed to surface and it is located sufficiently well within the sedimentary basin and far away from the high resistive SPL. Secondly, this proposed location is also fairly close to the Violeta well. Although the sediments are exposed to the surface at the SE end of AA' profile, this region is not advisable for drilling as it is very close to the SPL and thus the presence of fragments of hard rocks of SPL buried underneath, may hinder successful drilling.

It is important to note that although the region between gb03 and gb13 stations is feasible for drilling, identification of a precise location for drilling will be difficult, as the distance between these two stations is about 1 km. Therefore, a detailed electrical resistivity sounding survey with a dense network of measuring sites between these two

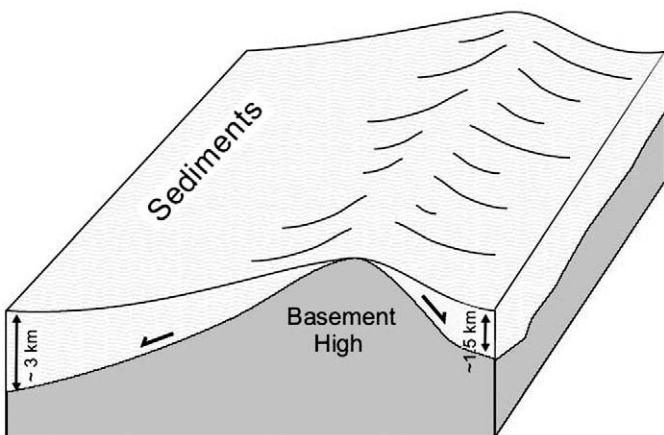


Fig. 10. A schematic of the inferred subsurface geological model based on the derived geoelectric models.

stations would be quite promising and worthwhile. A successful exploration of groundwater from any proposed drilling site(s) between gb03 and gb13 stations that would emerge out of this exercise could facilitate better assessment of water yield and subsequent viable options for the next major exercise of interlinking of the high yield Violeta well and the mapped aquifer zone. After all, the total quantity of water found in target area is strongly considered to be one of the key factors to determine the size of the village and surrounding areas for further development, agriculturally and otherwise in the semi-arid NE Brazil.

Acknowledgments

We thank the Conselho Nacional de Desenvolvimento Científico e Tecnológico (CNPq) of Brazil for financial support. One of the authors (EC) thanks CNPq for awarding him the Visiting Scientist fellowship at Observatorio Nacional, Brazil. We thank Emmanuele F. Lateral, Carlos Roberto Germano, Robinson Antonio dos Santos Almeida and Roberto da Silva Perreira for providing us with high quality MT data. We earnestly thank the editor and three anonymous referees for their meticulous reviews and constructive criticisms, which have greatly improved the paper. Discussions with T. Harinarayana have helped us a lot and we acknowledge the same with thanks. We thank Manoel Marques Maciel for his help in drawing Fig. 2. We thank Alan Jones for providing us with the *strike* program of McNeice and Jones. EC thanks S.C. Patel for stimulating discussions on the aquifer formations and help in the interpretation and Praveen Kumar for help in drawing some figures. EC expresses his sincere thanks to IRCC of IIT Bombay for providing partial financial assistance in the final stages of this work, through project 04IRO20. Finally, EC wishes to express his deep gratitude to all the staff of Observatorio Nacional, who have extended their kind cooperation and help on all the matters, administrative or otherwise, throughout his stay there and made his life pleasant and comfortable.

References

- Babiker, M., Gudmundsson, A., 2004. The effects of dykes and faults on groundwater flow in an arid land: the Red Sea Hills, Sudan. *Journal of Hydrology* 297, 256–273.
- Beamish, D., Travassos, J.M., 1992. A study of static shift removal from magnetotelluric data. *Journal of Applied Geophysics* 29, 157–178.
- Chouteau, M., Krivochieva, S., Rodriguez-Castillo, R., Gonzales-Morin, T., Jouanne, V., 1994. Study of the Santa Catarina aquifer system (Mexico Basin) using magnetotelluric soundings. *Journal of Applied Geophysics* 31, 85–106.
- Cunha, F.M.B., 1986. Evolucao paleozoica da Bacia do Parnaiba e seu arcabouco tectonico: MS thesis, Federal University, Rio de Janeiro, Brazil.
- de Brito Neves, B.B., 1991. Os dois 'Brasis' geotectonicos in simpósio de Geologia do Nordeste, 15, Recife-PE, SGB-NE, 1991, Boletim 12 da SGB-NE, p. 6.
- de Sousa, M.A., 1996. Regional gravity modelling and geohistory of the Parnaiba basin, Ph.D. Thesis, Dept. of Physics, Univ. of New Castle upon Tyne, UK.
- Egbert, G.D., 1997. Robust multiple station magnetotelluric data processing. *Geophysical Journal International* 130, 475–496.
- Fetter, C.W., 2001. *Applied Hydrogeology*, Fourth ed. Prentice Hall, NJ, USA.
- Fitterman, D.V., Stewart, M.T., 1986. Transient electromagnetic sounding for groundwater. *Geophysics* 51, 995–1005.
- Giroux, B., Chouteau, M., 1997. Use of magnetotelluric method in the study of the deep Maestrichian aquifer in Senegal. *Journal of Applied Geophysics* 38, 77–97.
- Goes, A.M.O., Travassos, W.A.S., Nunes, K.C., 1993. Projeto Parnaiba: Reavaliacao e perspectivas exploratorias: Relatório Petrobras, DEXNOR-DINTER.
- Groom, R.W., Bailey, R.C., 1989. Decomposition of the magnetotelluric impedance tensor in the presence of local three-dimensional galvanic distortions. *Journal of Geophysical Research* 94, 1913–1925.
- Groom, R.W., Kurtz, R.D., Jones, A.G., Boerner, D.E., 1993. A quantitative methodology for determining the dimensionality of conductivity structure from magnetotelluric data. *Geophysical Journal International* 115, 1095–1118.
- Jones, A.G., 1988. Static shift of magnetotelluric data and its removal in a sedimentary basin environment. *Geophysics* 53, 967–978.
- Krivochieva, S., Chouteau, M., 2003. Integrating TDEM and MT methods for characterization and delineation of the Santa Catarina aquifer (Chalco Sub-Basin, Mexico). *Journal of Applied Geophysics* 52, 23–43.
- McNeice, G.W., Jones, A.G., 2001. Multisite, multifrequency tensor decomposition of magnetotelluric data. *Geophysics* 66 (1), 158–173.
- McNeill, J.D., 1987. Advances in geomagnetic methods for groundwater studies. *Proceedings Exploration.-87. Applications of Geophysics and Geochemistry* 678–702.
- Meeke, J.A.C., Van Will, M.E.B., 1991. Comparison of seismic reflection and combined TEM/VES methods for hydrogeological mapping. *First Break* 9, 545–551.
- Meju, M., 1996. Joint inversion of TEM and distorted MT soundings: Some effective practical considerations. *Geophysics* 61, 56–65.
- Meju, M., Fontes, S.L., 1996. An investigation of dry water well near Floriano in northeast Brazil using combined VES/TEM/EMAP techniques. *Proceedings of the 8th EEGS symposium on application of Geophysics to Engineering and Environmental problems*, pp. 353–362.
- Meju, M.A., Fontes, S.L., Oliveira, M.F.B., Lima, J.P.R., Uluggerli, E.U., Carrasquilla, A.A., 1999. Regional aquifer mapping using combined VES-TEM-AMT/EMAP methods in the semi-arid eastern margin of Parnaiba Basin, Brazil. *Geophysics* 64 (2), 337–356.
- Ogawa, Y., 2002. On two-dimensional modelling of magnetotelluric field data. *Surveys in Geophysics* 23, 251–273.
- Palacky, G.J., Ritsema, I.L., De Jong, S.J., 1981. Electromagnetic prospecting for groundwater in Precambrian terrains in the republic of Upper Volta. *Geophysical Prospecting* 29, 932–955.
- Pellerin, L., Hohmann, G.W., 1990. Transient electromagnetic inversion: a remedy for magnetotelluric static shifts. *Geophysics* 55, 1242–1250.
- Rajaram, M., 2003. Multi-platform imaging of lithospheric magnetic anomalies. *Memoir Geological Society of India* 53, 233–245.
- Reid, A.B., Allsop, J.M., Granser, H., Miliett, A.J., Somerton, W.I., 1990. Magnetic interpretations in three dimensions using Euler deconvolution. *Geophysics* 55, 80–91.
- Rodi, W., Mackie, R.L., 2001. Non-linear conjugate gradients algorithm for 2-D magnetotelluric inversion. *Geophysics* 66, 174–187.
- Roest, W.E., Verhoef, J., Pilkington, M., 1992. Magnetic interpretation using 3-D analytic signal. *Geophysics* 57, 116–125.
- Sandberg, S.K., 1993. Examples of resolution of improvement in geoelectrical soundings applied to groundwater investigation. *Geophysical Prospecting* 41, 207–227.
- Schobbenhaus, C., et al., 1975. Carta geologica do Brasil ao Milionesimo, Folha Goias (SD.22); Brasília-DF, MME/DGM/DNPM, p. 114.
- Singer, B.Sh., 1992. Correction for distortions of magnetotelluric fields: limits of validity of the static approach. *Surveys in Geophysics* 13, 309–340.
- Sternberg, B.K., Washburne, J.C., Pellerin, L., 1988. Correction for the static shift in magnetotellurics using transient electromagnetic soundings. *Geophysics* 53, 1459–1468.
- Stewart, M.T., 1982. Evaluation of electromagnetic methods for rapid mapping of salt water interfaces in coastal aquifers. *Ground Water* 20, 538–545.
- Thompson, D.T., 1982. EULDPH – a new technique for making computer-assisted depth estimates from magnetic data. *Geophysics* 47, 31–37.
- Vozoff, K., 1991. In: Nabighian, M.N. (Ed.), *The Magnetotelluric Method. Electromagnetic Methods in Applied Geophysics*, vol. 2, pp. 641–711.